

# Current MD forcefields fail to capture key features of protein structure and fluctuations: A case study of cyclophilin A and T4 lysozyme

Zhe Mei<sup>1,2</sup>, Alex T. Grigas<sup>2,3</sup>, John D. Treado<sup>2,4</sup>, Gabriel Melendez Corres<sup>5</sup>, Maisa Vuorte<sup>6</sup>, Maria Sammalkorpi<sup>6,7</sup>, Lynne Regan<sup>8</sup>, Zachary A. Levine<sup>2,9,10</sup>, and Corey S. O’Hern<sup>2,4,11,12</sup>

<sup>1</sup>*Department of Chemistry, Yale University, New Haven, Connecticut, 06520, USA*

<sup>2</sup>*Integrated Graduate Program in Physical and Engineering Biology, Yale University, New Haven, Connecticut, 06520, USA*

<sup>3</sup>*Graduate Program in Computational Biology and Bioinformatics, Yale University, New Haven, Connecticut, 06520, USA*

<sup>4</sup>*Department of Mechanical Engineering and Materials Science, Yale University, New Haven, Connecticut, 06520, USA*

<sup>5</sup>*Department of Biology, UPR Humacao, Humacao, Puerto Rico 00792*

<sup>6</sup>*Department of Chemistry and Materials Science, School of Chemical Engineering, Aalto University, Aalto, Finland*

<sup>7</sup>*Department of Bioproducts and Biosystems, School of Chemical Engineering, Aalto University, Aalto, Finland*

<sup>8</sup>*Institute of Quantitative Biology, Biochemistry, and Biotechnology, Center for Synthetic and Systems Biology, School of Biological Sciences, University of Edinburgh, Edinburgh, UK*

<sup>9</sup>*Department of Pathology, Yale School of Medicine, New Haven, Connecticut, 06520, USA*

<sup>10</sup>*Department of Molecular Biophysics and Biochemistry, Yale University, New Haven, Connecticut, 06520, USA*

<sup>11</sup>*Department of Physics, Yale University, New Haven, Connecticut, 06520, USA*

<sup>12</sup>*Department of Applied Physics, Yale University, New Haven, Connecticut, 06520, USA*

**Abstract:** Globular proteins undergo thermal fluctuations in solution, while maintaining an overall well-defined folded structure. In particular, studies have shown that the core structure of globular proteins differs in small, but significant ways when they are solved by x-ray crystallography versus solution-based NMR spectroscopy. Given these discrepancies, it is unclear whether molecular dynamics (MD) simulations can accurately recapitulate protein conformations. We therefore perform extensive MD simulations across multiple force fields and sampling techniques to investigate the degree to which computer simulations can capture the ensemble of conformations observed in experiments. By analyzing fluctuations in the atomic coordinates and core packing, we show that conformations sampled in MD simulations both move away from and sample a larger conformational space than the ensemble of structures observed in NMR experiments. However, we find that adding inter-residue distance restraints that match those obtained via Nuclear Overhauser Effect measurements enables the MD simulations to sample more NMR-like conformations, though significant differences between the core packing features in restrained MD and the NMR ensemble remain. Given that the protein structures obtained from the MD simulations possess smaller and less dense protein cores compared to those solved by NMR, we suggest that future improvements to MD forcefields should aim to increase the packing of hydrophobic residues in protein cores.

## 1 Introduction

Over the past 50 years, numerous experiments have characterized the three-dimensional structure of globular proteins. For example, there are tens of thousands peptide and protein structures that have been solved by x-ray crystallography with resolutions less than 2 Å [1, 2]. In addition, ensembles of structures from more than ten thousand peptides and proteins have been obtained using solution NMR spectroscopy, providing complimentary information to existing crystal structures.

While the application of deep learning methods have improved protein structure predictions [3–5], it remains difficult to accurately predict the folded structure of a protein based solely on its sequence. One of the most frequently used methods for predicting protein structure and fluctuations is all-atom molecular dynamics (MD) simulations. Although a large number of peptides have been folded by MD simulations [6–10], only  $\lesssim 20$  distinct proteins have been successfully folded starting from non-native conformations using MD simulations. In smaller proteins (with  $N \lesssim 50$  residues), MD folding simulations often recapitulate the experimental structures with  $C_\alpha$  root-mean-square deviations (RMSD) less than 1.5 Å between the computational and experimental structures. However, for larger proteins between  $\sim 50$  and 80 amino acids, predictions from MD simulations yield backbones that deviate from experimental structures by more than 3.0 Å. (See Appendix 4.4 for a review of recent computational studies of protein folding.)

While prior protein folding simulations have been evaluated across multiple commonly used MD forcefields and for the ability of peptides and proteins to sample specific conformations, few studies have systematically characterized how fluctuations around the folded state in the MD simulations compare to fluctuations in experimental ensembles. For example, in x-ray crystal structures, one can define an ensemble from proteins that have been crystallized multiple times at high resolution. Such duplicates possess an average backbone RMSD  $\sim 1.0$  Å, which is consistent with the backbone RMSD values obtained from B-factors [11]. Alternatively, thermal fluctuations of proteins in solution can be described by high-quality NMR ensembles, where each model has more than 15-20 restraints per residue. In particular, the intra-bundle backbone RMSD for NMR ensembles plateaus beyond 15-20 restraints per residue at  $\sim 1.4$  Å [11]. Global backbone fluctuations generated from prior MD simulations of globular proteins (at room temperature) are larger than the fluctuations around the folded state observed in both x-ray crystallography and solution NMR experiments [11, 12]. (See Appendix 4.4.) These previous results emphasize the necessity for a systematic comparison of both local and global fluctuations in protein structure across multiple MD forcefields to determine their ability to recapitulate the fluctuations in the experimentally-derived NMR ensembles.

Prior computational studies have also considered whether experimentally-derived protein structures remain stable or deviate from their experimental conformations when they are used as initial structures in MD simulations across a wide range of atomistic forcefields. For example, in recent work by Robustelli, *et al.*, MD simulations initialized with NMR or x-ray crystal structures of small proteins were run for hundreds of  $\mu$ s, and their  $^3J$ -couplings, inter-residue distances from Nuclear Overhauser Effect (NOE) measurements, and residual dipolar couplings (RDCs) were compared to experimental values [13]. The authors found that the Amber99SB-ILDN forcefield yielded the most stable simulations and the closest agreement with NMR measurements. Thus, one might conclude that MD simulations using contemporary forcefields generally maintain experimentally-determined protein structures. While it is significant that many small proteins do not partially unfold during long MD simulations, this result does not imply that the conformational fluctuations sampled during the MD simulations are accurate, especially for core residues in large proteins. Both the fluctuations of residues on the surface and in the core obtained from MD simulations need to be compared quantitatively to those observed in spectroscopic experiments, such as NMR.

Recently, we showed that the packing of core residues in globular proteins dictates the quality of computational models, and that a failure to correctly pack core residues results in poorly folded model structures [14]. Therefore, systematic comparisons of molecular forcefields should also include studies of the important features of protein cores, including their fluctuations. The cores of experimentally-determined protein structures share several key properties, including (1) the fraction of residues that are core (defined by a relative solvent accessible surface area  $rSASA < 10^{-3}$ ) is typically between 5 – 10%, (2) the packing fraction  $\phi$  (fraction of space occupied by protein atoms) of core residues occurs between  $0.54 < \phi < 0.59$ , and (3) the atomic overlap among core residues is small, typically less than 0.1 Å per residue. We have previously shown that it is possible to distinguish ‘good’ (with small  $C_\alpha$  RMSD compared to experimental structures) from ‘bad’ computational models by determining whether the models satisfy the above three core packing properties. These results demonstrate the strong correlation between core structure and the conformation of the entire protein. Furthermore, high-quality protein structures deduced both through x-ray crystallography and NMR spectroscopy reveal that the NMR structures possess higher packing fractions in the core ( $\phi \sim 0.59$ ), even though the total core overlap energy and quality of side chain repacking is the same for x-ray crystal and NMR structures [11]. Subtle differences in core properties are important for determining the structure of the entire protein, and therefore should be included when analyzing protein conformations generated by MD simulations.

The prior results discussed above raise an important question. Since high-quality NMR and x-ray crystal structures possess differences in their backbone RMSD and core packing properties, do MD simulations generate protein conformations and fluctuations that are more similar to NMR or x-ray crystal structures?

To address this question, we carry out all-atom MD simulations of two well-resolved globular proteins with experimentally-determined x-ray and NMR structures, cyclophilin A [15] and T4 lysozyme\* [16], each containing  $N > 160$  residues. We evaluate fluctuations in their structure using three commonly used forcefields (CHARMM36m [17], Amber99SB-ILDN [18, 19], and Amber99SBNMR-ILDN [20]) to determine whether each can properly recapitulate core packing features of crystal structures or NMR bundles. Amber99SB-ILDN was developed to match secondary structure propensities found in experiments, Amber99SBNMR-ILDN was developed to incorporate NMR measurements, such as chemical shifts and  $J$ -couplings, and CHARMM36m was developed to sample diverse backbone conformations in folded and disordered proteins. We find that the cores of both proteins (in terms of  $C_\alpha$  RMSD, packing fraction, and fraction of core residues) are far more similar to those found in x-ray crystal structures than those in NMR bundles. Further, all three forcefields fluctuate with a global  $C_\alpha$  RMSD (relative to the x-ray crystal structure or the NMR bundle)  $\sim 3$  Å, which is larger than the fluctuations that occur in both x-ray crystal structure duplicates and within NMR bundles. By adding restraints among core residues based on NOE measurements from NMR experiments to the MD simulations, we can largely reduce the global  $C_\alpha$  RMSD (relative to the NMR bundle) in the MD simulations as expected. However, the global  $C_\alpha$  RMSD is still larger than the value measured from the NMR bundle. Thus, our results indicate that these MD forcefields are unable to capture experimentally measured NMR fluctuations. We also performed replica exchange MD (REMD) simulations to determine if accelerated sampling of the forcefields improves both the sampling of experimentally-determined structures and their fluctuations. We find that the structures sampled in the REMD simulations also do not possess the core packing properties of experimentally-determined NMR structures.

## 2 Results

In this work, we describe all-atom molecular dynamics simulations in explicit solvent of two proteins in an explicit solvent that were initialized with their experimental structures (either an x-ray crystal structure or one of the structures from the NMR bundle) using three of the most commonly used molecular forcefields, Amber99SB-ILDN, Amber99SBNMR-ILDN, and CHARMM36m. We chose to study the two globular proteins, cyclophilin A and T4 lysozyme\*, because they both have been experimentally-determined to high resolution using x-ray crystallography and with a large number of restraints using NMR spectroscopy. (See Sec. 4.2 for descriptions of the two proteins used in this study.) After initializing the MD simulations with the experimentally-determined structures, we ran long trajectories ( $\geq 1\mu\text{s}$ ), and measured the  $C_\alpha$  RMSD with respect to the NMR and x-ray crystal structures, the fraction of core residues, their packing fractions, and related structural quantities as a function of time. (As a comparison, the global  $C_\alpha$  RMSD from previous MD studies of folding and stability are presented in Appendix 4.4.) The MD simulations were carried out at room temperature, 1 bar of pressure, and in a large cubic box with periodic boundary conditions. (See Sec. 4 for a detailed description of the methodology employed for the MD simulations.)

To calibrate the results of the MD simulations, we must first determine the conformational fluctuations in globular proteins in experiments. We previously identified a set of over 20 proteins that have been characterized multiple times by x-ray crystallography to a resolution of  $< 2$  Å and by NMR using  $> 15$ -20 restraints per residue [11]. First, for a given protein, do duplicate x-ray crystal structures and structures from the NMR bundle fluctuate around the same average structure? Second, is the magnitude of these fluctuations between x-ray duplicates and NMR ensembles the same? We found that, in general, the fluctuations in structure in the NMR ensemble are larger than those for the x-ray duplicate ensemble, and the difference in the average structure between the x-ray and NMR ensembles is larger than the fluctuations within each ensemble separately. For example, for core residues, we found that the average  $C_\alpha$  RMSD of core residues among x-ray crystal structure duplicates is  $\approx 0.1$  Å, the average  $C_\alpha$  RMSD of core residues among models within each NMR bundle is  $\approx 0.5$  Å, and the average  $C_\alpha$  RMSD of core residues between the x-ray duplicates

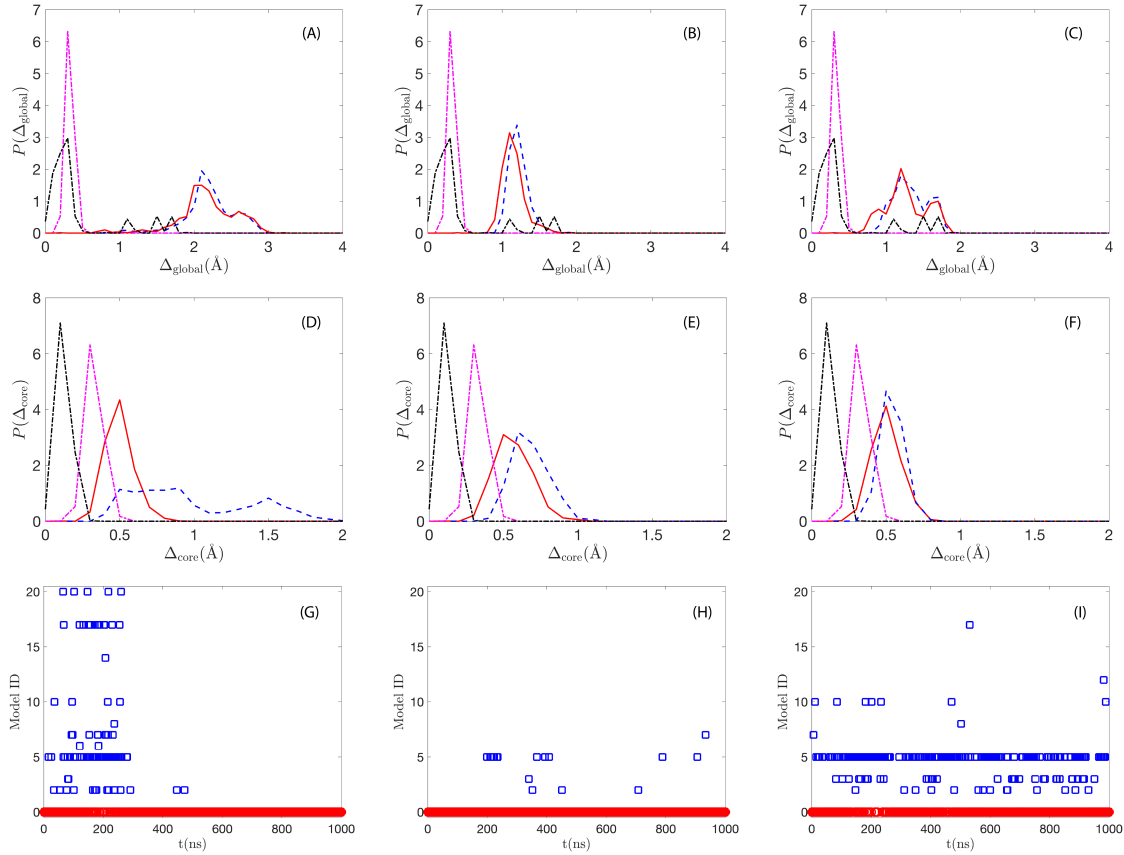


Figure 1: Structural fluctuations of cyclophilin A from all-atom MD simulations and experimentally-determined x-ray crystal and solution-based NMR structures. The three columns provide results for the all-atom MD simulations using the (left) CHARMM36m, (middle) Amber99SB-ILDN, and (right) Amber99SBNMR-ILDN, forcefields. (A)-(C) The probability distributions  $P(\Delta_{\text{global}})$  of the root-mean-square deviations  $\Delta_{\text{global}}$  in the positions of the  $C_{\alpha}$  atoms of all residues in the protein [in Å] between structures in the NMR bundle (magenta dot-dashed lines), between the x-ray crystal structure duplicates (black dot-dashed lines), between the structures in the MD simulations and the closest x-ray duplicates (red solid lines), and between the structures in the MD simulations and closest models in the NMR bundle (blue dashed lines). (D)-(F) The probability distributions  $P(\Delta_{\text{core}})$  of the root-mean-square deviations  $\Delta_{\text{core}}$  in the positions of the  $C_{\alpha}$  atoms of the core residues [in Å] for the same data in panels (A)-(C). (G)-(I) The identification number of the NMR or x-ray crystal structure with the smallest  $\Delta_{\text{core}}$  with respect to the MD structure at each time  $t$ . Model 0 corresponds to the x-ray crystal structure with PDB code 3k0m, and models 1-20 indicate the NMR models in the bundle ordered from smallest to largest  $\Delta_{\text{core}}$  relative to the x-ray crystal structure with PDB code 3k0m. The MD simulations in (A)-(I) were initialized using the x-ray crystal structure with PDB code 3k0m.

and models in each NMR bundle is  $\approx 0.8$  Å. (We define core residues as those with sufficiently small relative solvent accessible surface area, rSASA. See Sec. 4 for the definitions of rSASA and RMSD.) We also characterized the global fluctuations. We found that the average global  $C_\alpha$  RMSD among the x-ray crystal structure duplicates is  $\approx 0.5$  Å, the average global  $C_\alpha$  RMSD among models within each NMR bundle is  $\approx 1.2$  Å, and the average global  $C_\alpha$  RMSD between the x-ray duplicates and models in each NMR bundle is  $\approx 1.8$  Å. The differences (both for core residues and globally) between the structures in the x-ray crystal and NMR ensembles are substantially larger than the fluctuations within each ensemble separately.

Both cyclophilin A and T4 lysozyme\* are examples from the dataset of proteins that have duplicate high-resolution x-ray crystal structures and high-quality NMR structures. First, we will discuss the results for cyclophilin A. In Fig. 1, we show that the average core  $C_\alpha$  RMSD among the x-ray crystal structure duplicates is  $\approx 0.1$  Å and among models within the NMR bundle is  $\approx 0.3$  Å. The average global  $C_\alpha$  RMSD among the x-ray crystal structure duplicates is  $\approx 0.4$  Å and among the models within the NMR bundle is  $\approx 0.5$  Å. We compare these results to those from MD simulations starting from an x-ray duplicate structure (with PDB code 3k0m). In Fig. 1 (A)-(C), we show the distributions  $P(\Delta_{\text{global}})$  of the  $C_\alpha$  RMSD for all residues in cyclophilin A among x-ray duplicates, among models in the NMR bundle, between structures in the MD simulations and the closest x-ray duplicates, and between structures in the MD simulations and the closest models in the NMR bundle for the three MD forcefields. For all forcefields,  $P(\Delta_{\text{global}})$  is shifted to larger values for the MD simulations compared to  $P(\Delta_{\text{global}})$  for the experimentally-determined x-ray duplicate and NMR ensembles.

Similar results are found for the distribution  $P(\Delta_{\text{core}})$  of  $C_\alpha$  RMSD for core residues in Fig. 1 (D)-(F) obtained from MD simulations of cyclophilin A. For all three forcefields,  $P(\Delta_{\text{core}})$  is shifted to larger values for the MD simulations compared to  $P(\Delta_{\text{core}})$  for the experimentally-determined x-ray duplicate and NMR ensembles. In panel (D), we find that  $P(\Delta_{\text{core}})$  is particularly broad for the MD simulations with CHARMM36m, extending to  $\Delta_{\text{core}} > 1.5$  Å where there is no weight in  $P(\Delta_{\text{core}})$  for the experimentally-determined NMR bundle. We find similar results for  $P(\Delta_{\text{global}})$  and  $P(\Delta_{\text{core}})$  for the MD simulations when they are initialized using models from the NMR bundle in Fig. 2. Similar results are found for MD simulations of cyclophilin A using the two Amber forcefields in Appendix 4.4. Thus, for all three forcefields tested in this study, the fluctuations,  $\Delta_{\text{global}}$  and  $\Delta_{\text{core}}$ , observed in MD simulations for cyclophilin A are in general larger than those observed in the experimentally-determined x-ray duplicate and NMR ensembles. These results show that the MD simulations of cyclophilin A sample a broader set of structures than either the x-ray duplicate or NMR ensembles.

We also investigated whether the structures sampled in the MD simulations are closer (determined by the smallest  $C_\alpha$  RMSD,  $\Delta_{\text{core}}$ , for core residues) to a particular structure in the x-ray duplicate or NMR ensembles. In Fig. 1 (G)-(I), we identify the particular structure (either the x-ray crystal structure with PDB code 3k0m, labelled 0, or one of 20 models in the NMR bundle, ordered from smallest to largest  $\Delta_{\text{core}}$  from the x-ray crystal structure) that is closest to the protein structure in the MD simulations as a function of time for each of the three forcefields. In general, the structures in the MD simulations are closer to the x-ray crystal structure than the models in the NMR bundle. The structures in the MD simulations are closer (minimum  $C_\alpha$  RMSD) to the x-ray crystal structure  $\approx 82\%$ ,  $97\%$ , and  $56\%$  of the time for CHARMM36m, Amber99SB-ILDN, and Amber99SBNMR-ILDN, respectively. For the MD simulations with Amber99SBNMR-ILDN, 8 of the 20 NMR model structures are sampled. One model is sampled the most, at 20% of the time.

In recent studies, we found that properties of core packing in globular proteins were different for protein structures obtained from x-ray crystallography and from solution NMR spectroscopy. In particular, we found that the packing fraction of core residues from high-resolution x-ray crystal structures was  $\langle \phi \rangle = 0.55 \pm 0.01$ , whereas  $\langle \phi \rangle = 0.59 \pm 0.02$  for structures obtained from NMR. Thus, an important question is whether the packing properties of protein cores generated from MD simulations more closely resemble those in x-ray crystal or NMR structures. In Fig. 3 (A)-(C), we show the probability distribution  $P(\phi, f_{\text{core}})$  for obtaining

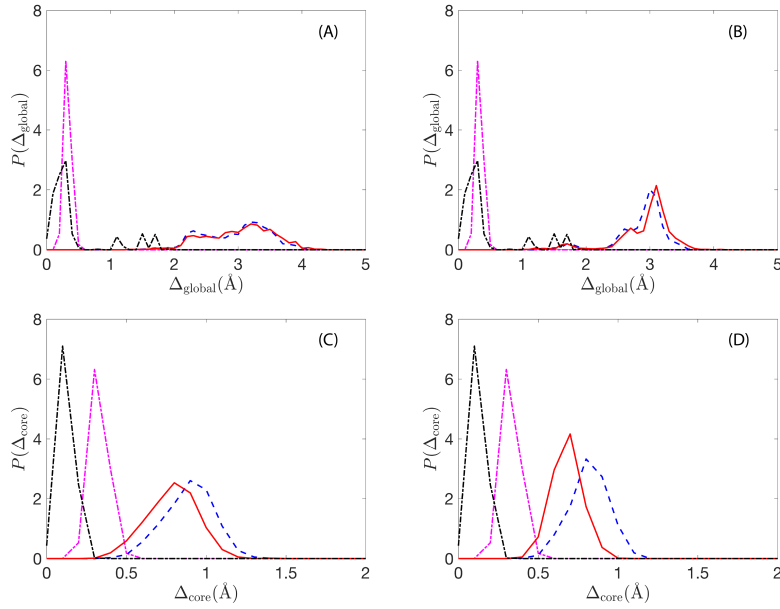


Figure 2: (A)-(B) The probability distributions  $P(\Delta_{\text{global}})$  of the root-mean-square deviations  $\Delta_{\text{global}}$  in the positions of the  $C_{\alpha}$  atoms of all residues in cyclophilin A [in Å] between structures in the NMR bundle (magenta dot-dashed lines), between the x-ray crystal structure duplicates (black dot-dashed lines), between the structures in the MD simulations (using CHARMM36m) and the closest x-ray duplicates (red solid lines), and between the structures in the MD simulations (using CHARMM36m) and the closest models in the NMR bundle (blue dashed lines). The MD simulations in (A) and (B) were initialized using two different models from the NMR bundle. (C)-(D) The probability distributions  $P(\Delta_{\text{core}})$  of the root-mean-square deviations  $\Delta_{\text{core}}$  in the positions of the  $C_{\alpha}$  atoms of the core residues [in Å] for the same data in panels (A) and (B).

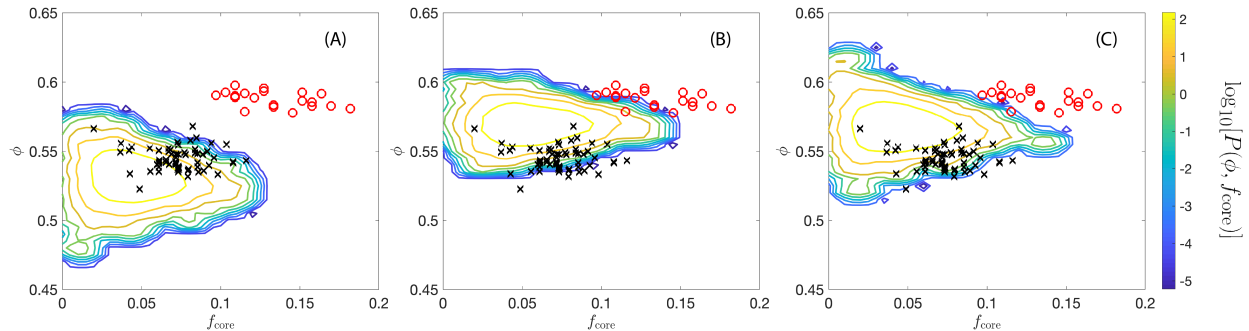


Figure 3: Probability distribution  $P(\phi, f_{\text{core}})$  of the packing fraction  $\phi$  of the core and fraction of core residues  $f_{\text{core}}$  from MD simulations of cyclophilin A using the (A) CHARMM36m, (B) Amber99SB-ILDN, and (C) Amber99SBNMR-ILDN forcefields. The contours are shaded using the color scale from yellow with high probability to dark blue with low probability. (The MD simulations were initialized in the x-ray crystal structure with PDB code 3k0m.) In addition to the results for each forcefield, we include values of  $\phi$  and  $f_{\text{core}}$  for the x-ray crystal structure duplicates (black exes) and all models in the NMR bundle (red open circles).

core packing fraction  $\phi$  and fraction of core residues  $f_{\text{core}} = N_c/N$ , where  $N_c$  is the number of core residues with  $\text{rSASA} < 10^{-3}$ , during MD simulations of cyclophilin A with each of the three forcefields. We compare  $P(\phi, f_{\text{core}})$  to the  $\phi$  and  $f_{\text{core}}$  values for each structure in the x-ray crystal structure duplicate and NMR dataset for cyclophilin A. As expected, the mean core packing fraction for the NMR structures for cyclophilin A,  $\langle \phi \rangle \sim 0.59$ , is larger than that for the x-ray crystal structure duplicates,  $\langle \phi \rangle \sim 0.54$ . Further, the mean fraction of core residues,  $\langle f_{\text{core}} \rangle \sim 0.13$ , is larger for the NMR structures of cyclophilin A compared to that for the x-ray crystal structure duplicates,  $\langle f_{\text{core}} \rangle \sim 0.07$ . For the MD simulations with CHARMM36m, the protein samples  $\phi$  and  $f_{\text{core}}$  values that are similar to, but slightly smaller than those for the x-ray crystal structures. For CHARMM36m, the protein never samples the NMR values of  $\phi$  and  $f_{\text{core}}$ . For the MD simulations using the Amber99SB-ILDN and Amber99SBNMR-ILDN forcefields,  $P(\phi, f_{\text{core}})$  shifts to larger values of  $\phi$  and  $f_{\text{core}}$ , but few of the NMR-determined values of  $\phi$  and  $f_{\text{core}}$  are sampled. Thus, the MD simulations of cyclophilin A for all three forcefields most frequently sample  $\phi$  and  $f_{\text{core}}$  values associated with the cores of x-ray crystal structures, not the cores of NMR structures. Note that while  $P(\phi, f_{\text{core}})$  samples x-ray crystal structures more often, the peak of  $P(\phi, f_{\text{core}})$  is not centered on the data for x-ray crystal structures.

For comparison, we also performed ( $\geq 1\mu\text{s}$ ) MD simulations of T4 lysozyme\* using the three forcefields and both the x-ray crystal and NMR structures as initial conditions. The results presented in Fig. 4 for MD simulations of T4 lysozyme\* are qualitatively similar to those presented in Figs. 1-3 for cyclophilin A. In particular, the core and global  $C_\alpha$  RMSD between the structures in the MD simulations and the experimentally-determined x-ray crystal and NMR structures are much larger than the respective RMSD measures for the x-ray duplicate and NMR ensembles separately. For example, as shown in Fig. 4 (A),  $\langle \Delta_{\text{global}} \rangle \sim 2.7\text{\AA}$  between structures in the MD simulations and the closest x-ray duplicates. In contrast,  $\langle \Delta_{\text{global}} \rangle = 0.4\text{\AA}$  for x-ray duplicate structures. Moreover, as shown in Fig. 4 (B),  $\langle \Delta_{\text{core}} \rangle \sim 0.8\text{\AA}$  between structures in the MD simulations and the closest x-ray duplicates, whereas  $\langle \Delta_{\text{global}} \rangle = 0.2\text{\AA}$  for x-ray duplicate structures for T4 lysozyme\*. In Fig. 4 (C), we show the probability distribution  $P(\phi, f_{\text{core}})$  from the MD simulations of T4 lysozyme\*. Although the  $\phi$  and  $f_{\text{core}}$  values for the x-ray crystal and NMR structures are closer together for T4 lysozyme\* than for cyclophilin A, we still find that the MD simulations frequently sample smaller values of  $\phi$  and  $f_{\text{core}}$  than those found for the NMR structures.

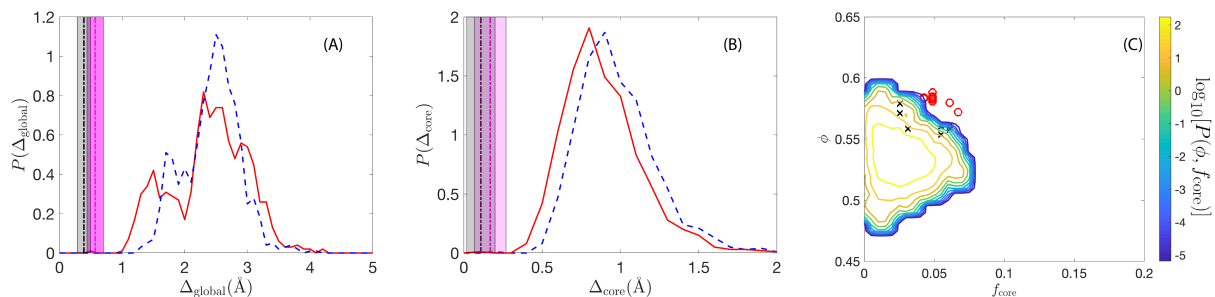


Figure 4: (A) Probability distribution  $P(\Delta_{\text{global}})$  for the  $C_{\alpha}$  RMSD for all residues in T4 lysozyme\* between the structures generated from MD simulations using CHARMM36m and the closest x-ray duplicates (red solid line) and the closest models in the NMR bundle (blue dashed line). We also show the mean and standard deviation for  $\Delta_{\text{global}}$  for the x-ray duplicate dataset (black dashed-dotted line indicates the mean and gray shaded region indicates the standard deviation) and NMR bundle (magenta dashed-dotted line indicates the mean and magenta shaded region indicates the standard deviation). In (B), we show results for  $P(\Delta_{\text{core}})$  for the same data in (A). We also show the mean and standard deviation for  $\Delta_{\text{core}}$  for the x-ray duplicate dataset (black dashed-dotted line indicates the mean and gray shaded region indicates the standard deviation) and NMR bundle (magenta dashed-dotted line indicates the mean and magenta shaded region indicates the standard deviation). (C) Probability distribution  $P(\phi, f_{\text{core}})$  of the packing fraction  $\phi$  of the core and fraction of core residues  $f_{\text{core}}$  from MD simulations of T4 lysozyme\* using CHARMM36m. The contours are shaded using the color scale from yellow with high probability to dark blue with low probability on a logarithmic scale. We also include values of  $\phi$  and  $f_{\text{core}}$  for the x-ray duplicates (black crosses) and all models in the NMR bundle (red open circles). (The MD simulations for T4 lysozyme\* were initialized in the x-ray crystal structure with PDB code 3dmv.)



In the studies described above, we started the MD simulations with experimentally-determined NMR and x-ray crystal structures as the initial conditions, ran the MD simulations for  $1\mu\text{s}$ , and showed that multiple MD forcefields sample conformations that are closer to the x-ray crystal structures compared to NMR structures. In addition, all three forcefields failed to sample cores that are as large and densely packed as those in the NMR bundle. In Appendix 4.4, we describe tests of convergence of the RMSD and radius of gyration as a function of time during the MD simulations. We show that the  $1\mu\text{s}$  MD simulations with the Amber forcefields do not change with time beyond  $\sim 100\text{ns}$ . However, for the MD simulations of cyclophilin A using the CHARMM36m forcefield, the  $C_\alpha$  RMSD and radius of gyration increase with time, and thus we stopped the MD simulations with CHARMM36m at  $1\mu\text{s}$  and instead used an enhanced sampling technique to explore the forcefield further.

To determine whether the differences in structure and fluctuations between the MD simulations and NMR experiments are, at least in part, due to under-sampling of experimental conformations, we enhanced the sampling of the MD simulations using a replica exchange protocol. If increased computational sampling moves the MD simulations closer to the NMR ensemble, under-sampling is likely occurring. However, if conformations continue to diverge from the NMR ensemble, it is likely that the forcefield possesses low-lying energy minima that are distinct from those in the experimental ensemble. Thus, we performed replica exchange molecular dynamics (REMD) simulations of cyclophilin A to further explore low-energy protein conformations that are sampled by the CHARMM36m forcefield. For the REMD simulations, we considered a partially unfolded initial structure that was prepared at elevated temperatures with  $R_g/R_g^0 > 2$  (where  $R_g^0$  is the radius of gyration of the x-ray crystal structure) and core  $C_\alpha$  RMSD  $\Delta_{\text{core}} \approx 1.5\text{\AA}$  compared to the x-ray crystal structure and nearest NMR structure, which is much larger than core  $C_\alpha$  RMSD values among the x-ray crystal structure duplicates or NMR bundle. Initializing the REMD simulations with a partially unfolded structure allows us to determine whether the REMD simulations can find the correct folded structure of cyclophilin A when they are started in a protein structure from a region of conformation space that is distant from the experimentally-determined structures. (See Sec. 4 for a detailed discussion of the REMD simulation methodology.)

We show in Fig. 5 (A) that MD simulations started from the partially unfolded structure remain far from the experimental x-ray crystal structure. In particular, the distribution  $P(\Delta_{\text{core}})$  of core  $C_\alpha$  RMSD values (relative to the x-ray crystal structure PDB: 3k0m) for the MD simulations starting from the partially unfolded structure is peaked at  $\Delta_{\text{core}} \sim 2.2\text{\AA}$ , whereas it is peaked at  $\Delta_{\text{core}} \sim 0.5\text{\AA}$  when the starting structure is the x-ray crystal structure with PDB code 3k0m. In contrast, when we initialize the REMD simulations with the partially unfolded structure,  $P(\Delta_{\text{core}})$  is broad, sampling structures over a range of  $\Delta_{\text{core}}$  from  $0.75\text{\AA}$  to greater than  $5\text{\AA}$  (relative to the x-ray crystal structure). Thus, REMD simulations, even though they are initialized with partially unfolded structures, are able to sample, albeit infrequently, structures that are close to (less than  $1\text{\AA}$ ) the x-ray crystal structure. Thus, the REMD protocol might be promising for protein structure prediction. However, one must be able to identify when the REMD simulation is close to the experimental structure, without knowing the experimental structure beforehand. The distance to the x-ray crystal structure can be estimated using protein decoy detection methods [14, 21–23], which have their own limitations, and would limit the ability of REMD to identify experimental conformations. It is likely that the CHARMM36m forcefield possesses low-lying energy minima that are distinct from those sampled by x-ray crystal structures.

We also investigate whether these REMD simulations started from a partially unfolded structure sample conformations that are close to the NMR structures for cyclophilin A. In Fig. 5 (B), we first divide the REMD simulation ( $10^4$  frames) into 136 clusters, where each pair of structures within each cluster has  $\Delta_{\text{core}} < 1\text{\AA}$ . We then calculate the average core  $C_\alpha$  RMSD  $\Delta_{\text{core}}$  between the structures in each cluster and the nearest structure in the NMR bundle. In Fig. 5 (B), we plot  $\Delta_{\text{core}}$  versus the cluster label, where the clusters are ordered based on the number of REMD frames in each. Overall, most of the REMD clusters have large

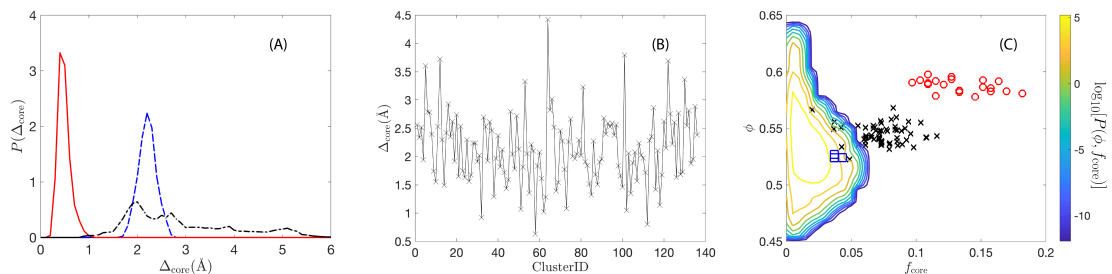


Figure 5: (A) Probability distributions of the core  $C_\alpha$  RMSD  $\Delta_{\text{core}}$  (relative to the x-ray crystal structure PDB code 3k0m) from MD simulations (at room temperature using CHARMM36m) of cyclophilin A starting from the x-ray crystal structure with PDB code 3k0m (red solid line) and starting from the x-ray crystal structure heated to a temperature above the unfolding temperature (blue dashed line). We also show  $\Delta_{\text{core}}$  from REMD simulations (at room temperature) starting from the same structure prepared at elevated temperature (black dot-dashed line). (B) The average core  $C_\alpha$  RMSD  $\langle \Delta_{\text{core}} \rangle$  (relative to the closest NMR structure) obtained from REMD simulations of cyclophilin A at room temperature starting from the structure prepared at elevated temperature. The REMD structures obtained from  $10^4$  snapshots separated by 200 ns were grouped into 136 clusters for which any two structures possess  $\Delta_{\text{core}} < 1\text{\AA}$ . (C) Probability distribution  $P(\phi, f_{\text{core}})$  of the packing fraction  $\phi$  of the core and fraction of core residues  $f_{\text{core}}$  from the REMD simulations described in (A) and (B). The contours are shaded using the color scale from yellow with high probability to dark blue with low probability on a logarithmic scale. We also include values of  $\phi$  and  $f_{\text{core}}$  for the x-ray crystal structure duplicates (black crosses) and all models in the NMR bundle (red open circles) for cyclophilin A. The three open squares indicate the average values of  $\phi$  and  $f_{\text{core}}$  for clusters 31, 57, and 111 from (B).

$\Delta_{\text{core}}$  compared to the closest structure in the NMR bundle. However, three clusters (with cluster labels 31, 57, and 111) possess  $\Delta_{\text{core}} < 1\text{\AA}$  relative to the closest structure in the NMR bundle. In Fig. 5 (C), we plot the distribution  $P(f_{\text{core}}, \phi)$  for the REMD simulations starting from a partially unfolded structure and find that overall the packing properties of the structures in the REMD simulations are different than those found in the x-ray crystal and NMR structures. In fact,  $P(f_{\text{core}}, \phi)$  samples regions of large packing fraction  $0.58 < \phi < 0.65$  and small fraction of core residues  $0 < f_{\text{core}} < 0.025$  that were not sampled in the MD simulations of cyclophilin A initialized with the experimentally-determined structures. It is possible that the REMD simulations, which are seeded with conformations at higher temperatures, bias the system towards higher packing fractions as has been observed in MD simulations of jammed packings of amino acid-shaped particles [11]. The average packing fraction of core residues  $\phi$  and fraction of core residues  $f_{\text{core}}$  for clusters 31, 57, and 111 are closer to the values for x-ray crystal structures than for the NMR models. Even after exploring a broad region of conformation space, most favorable conformations in the REMD simulations do not possess core packing features that are similar to those in the NMR bundle.

We have demonstrated via several metrics (local and global  $C_{\alpha}$  RMSD, fraction of core residues, and packing fraction) that current MD forcefields (CHARMM36m, Amber99SB-ILD and Amber99SBNMR-ILDN) fail to recapitulate protein structure fluctuations in NMR bundles. One possible method for accurately simulating protein structure fluctuations would be to add harmonic restraints between atom pairs for which we have NOE measurements and other NMR data. For example, in the Biological Magnetic Resonance Bank (BMRB) [24], we find that there are a total of 4101 NOE atom pairs and 127 pairs involving atoms in core residues for which NOE measurements have been performed for cyclophilin A. (All of the restraints between core heavy atoms, 24 pairs, are listed in Appendix 4.6.) By adding harmonic restraints for the 127 atomic separations involving core residues (using spring constants that are comparable to those for covalently bonded atoms), we are able to reduce  $\Delta_{\text{core}}$  and  $\Delta_{\text{global}}$  as shown in Table 1. (See Sec. 4 for a description of the implementation of the harmonic restraints between atom pairs in the MD simulations.) The NMR bundle satisfies all of its core NOE restraints, as the models were fit to this data. The unrestrained MD simulations using the CHARMM36m forcefield only satisfy 49% of the core NOE restraints on average. The MD simulations with harmonic restraints using the CHARMM36m forcefield recapitulate  $\approx 73\%$  of the core NOE restraints. Thus, other competing forces in the CHARMM36m forcefield prevent the remaining atomic pair separations from satisfying the NOE restraints. There are at least two ways to improve the frequency with which the MD simulations satisfy the NOE distance measurements: increase the spring constant for the harmonic restraints among core NOE atom pairs or increase the number of restraints, for example, by including harmonic restraints between non-core and core NOE atom pairs. We did not increase the spring constant of the harmonic restraints above the values of carbon-carbon bonds because this can lead to unphysical stretching of covalent bonds. Adding more restraints yields an MD simulation methodology that must be tailored for each individual protein, and is not applicable to a broad set of globular proteins. We do not believe this is a fruitful approach.

In Fig. 6 (A) and (B), we show that the core and global  $C_{\alpha}$  RMSD distributions for the restrained MD simulations (orange dotted lines) are shifted to lower values compared to those for the unrestrained MD simulations for cyclophilin A. However, the RMSD distributions for the restrained simulations still yield larger RMSD values than those sampled by the structures in the NMR bundle. In addition, we find in Fig. 6 (C) that the packing fractions sampled by the restrained MD simulations are shifted upward relative to values for the unrestrained MD simulations (Fig. 3 (A)), but the fractions of the residues that are identified as core remains low,  $f_{\text{core}} < 0.1$ , whereas  $0.1 < f_{\text{core}} < 0.18$  for structures sampled by the NMR ensemble. While restraining core atomic separations can reduce the fluctuations of cyclophilin A, only constraining the core atomic separations is not sufficient for recapitulating the conformational fluctuations of cyclophilin A. The non-core region of the protein becomes less dense than the experimental structure and exposes the core region, which leads to low values of  $f_{\text{core}}$ . Future studies are needed to determine the number and type of atomic distance restraints that are needed to maintain the core properties of the NMR ensemble of structures

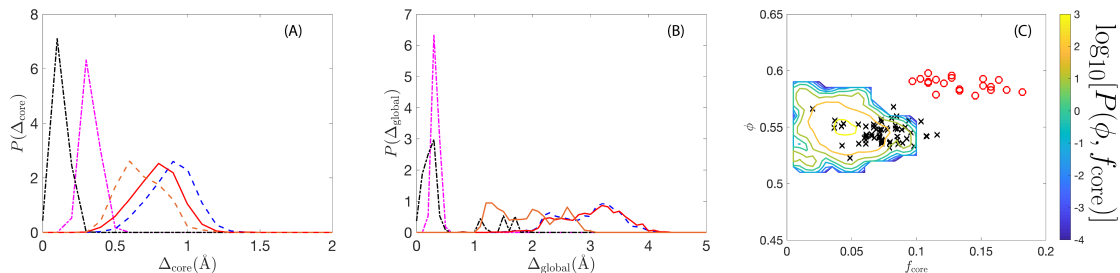


Figure 6: The probability distributions of the (A) global  $\Delta_{\text{global}}$  and (B) core RMSD  $\Delta_{\text{core}}$  of  $C_{\alpha}$  atoms between structures obtained from the restrained MD simulations of cyclophilin A (using CHARMM36m) compared to the NMR bundle (orange dashed line). We also show  $\Delta_{\text{global}}$  and  $\Delta_{\text{core}}$  for the x-ray crystal structure duplicates (black dot-dashed line), NMR bundle (magenta dot-dashed line), and for structures from the unrestrained MD simulations of cyclophilin A (CHARMM36m) compared to the NMR bundle (blue dotted line) and x-ray crystal structure duplicates (red solid line). (C) Probability distribution  $P(\phi, f_{\text{core}})$  of the packing fraction  $\phi$  of the core and fraction of core residues  $f_{\text{core}}$  from restrained MD simulations of cyclophilin A using CHARMM36m. We also show values of  $\phi$  and  $f_{\text{core}}$  from x-ray crystal structure duplicates (black crosses) and all models in the NMR bundle (red open circles). The contours are shaded using the color scale from yellow with high probability to dark blue with low probability on a logarithmic scale. (The MD simulations were initialized in the x-ray crystal structure with PDB: 3k0m.)

for cyclophilin A.

### 3 Discussion and Conclusions

We have seen in our previous studies that high-quality structures obtained from x-ray crystallography and NMR spectroscopy possess different distributions of the  $C_{\alpha}$  RMSD for core residues (e.g.  $\langle \Delta_{\text{core}} \rangle$  is larger for the NMR ensemble compared to that for x-ray crystal structure duplicates) and different core packing fractions and core sizes [11]. Possible explanations for these differences include the experimental conditions. For example, the crystalline environment and typical low temperatures used in x-ray scattering studies of proteins are different from the conditions for solution-based NMR spectroscopy carried out at room temperature. An important goal of MD simulations is to understand the stability of x-ray crystal structures when they are used as initial conditions in MD simulations with explicit solvent at room temperature. For example, do MD simulations initialized with x-ray crystal structures and run with explicit solvent at room temperature yield structures similar to those in the NMR ensemble or do they remain close to the x-ray crystal structure?

The goal of this article was to address this question using several quantities that characterize protein structure. We conducted long molecular dynamics simulations of two large proteins starting in different experimentally-determined structures using three commonly used forcefields. We found that the RMSD fluctuations of backbone  $C_{\alpha}$  atoms in the core and globally in the MD simulations to be both different in magnitude and character compared to the fluctuations in experimentally-determined structures. The conformations sampled in MD simulations are also closer to the x-ray crystal structures than the NMR structures, even when we use structures from the NMR bundle as initial conditions. Additionally, both the size and packing fraction of the cores generated in the MD simulations are more similar to those in x-ray crystal structures, while also sampling many conformations that are more solvent exposed than in x-ray structures. Overall, the MD simulations of these two proteins create smaller and less densely packed cores than those

found for structures in the NMR ensemble. Further sampling of CHARMM36m, via REMD simulations, did not generate conformations that are more similar to x-ray crystal or NMR structures. Finally, we showed that by adding harmonic NOE atomic distance restraints, we can reduce the core and global  $C_\alpha$  RMSD relative to the experimentally-determined structures, although further investigation is needed to identify a minimal set of atomic distance restraints that are needed to recapitulate the core structure.

In the Results section, we compared the atomic coordinates for the structures generated from the MD simulations and the experimental structures in the NMR ensemble. The atomic coordinates in the NMR bundle are obtained through a process of successively incorporating NMR measurements of scalar couplings, chemical shifts, residual dipolar couplings (RDC), NOE atomic separations, and others as restraints on the set of atomic coordinates. Other computational studies of protein folding and stability have compared their MD simulation results to primary NMR experimental data [13, 25–28]. (Note that even when comparing MD simulations to NMR measurements, one typically uses approximate classical methods to convert atomic coordinates into NMR measurements [29].) To compare our MD simulations to NMR measurements, we calculated the deviation  $Q_J$  of the  $^3J$ -couplings obtained from the MD simulations of cyclophilin A relative to the values from the NMR bundle. (See Fig. 7 (A) and Eq. 6 in Sec. 4.) Similar to our results above, the two Amber forcefields show smaller  $Q_J$  values for  $^3J$ -couplings than those for the CHARMM36m forcefield. This result agrees with previous MD simulation studies of smaller proteins [13]. However, the  $Q_J$  values from the MD simulations are at least a factor of 3 larger than those from the NMR measurements.

RDC data provides longer-range spatial information than  $^3J$ -couplings and, unlike NOE measurements, which give atomic separations, RDC data also provides information on the relative orientations of the bond vectors. For cyclophilin A, the  $^3J$ -couplings were used to determine the structures in the NMR bundle, whereas the RDC data was made available after the NMR bundle was released. We used the Prediction of Alignment from Structure (PALES) software to calculate the RDC values from the atomic coordinates of the NMR bundle and MD simulations [29]. The RDC data agrees with the structures in the NMR bundle (i.e.  $Q_{\text{RDC}} \sim 0.48$  [30, 31]), but not as closely as the  $^3J$ -couplings do ( $Q_J \sim 0.05$ ) [32]. In Fig. 7 (B), we show that the structures in the MD simulations possess  $Q_{\text{RDC}}$  values between 0.9 and 1.0, whereas  $\langle Q_{\text{RDC}} \rangle \sim 0.48$  for the NMR bundle. The  $Q_{\text{RDC}}$  values from the MD simulations are much larger than those previously reported for simulations of smaller proteins using similar forcefields [13, 28, 33]. By applying restraints on all measured  $^3J$ -couplings and NOE atomic separations in cyclophilin A, restrained MD simulations using a forcefield similar to Amber99SB-ILDN can sample conformations with  $Q_{\text{RDC}} \sim 0.3$  [32]. In contrast, the unrestrained MD simulations of cyclophilin A possess large  $Q_{\text{RDC}}$  values. Fig. 7 (B) further emphasizes the sensitivity of RDC values in MD simulations, since  $Q_{\text{RDC}}$  grows rapidly with  $\Delta_{\text{global}}$ .

Overall, we have seen across three state-of-the-art forcefields, CHARMM36m, Amber99SB-ILDN, and Amber99SBNMR-ILDN, that MD simulations of two large proteins starting from NMR structures, x-ray crystal structures, and a partially unfolded structure, do not adequately recapitulate numerous important properties of the NMR ensemble. In particular, the cores sampled in the MD simulations are smaller and less densely packed than structures in the NMR bundle. Not a single conformation sampled in the MD simulations captured features in the space of core packing fraction and fraction of core residues sampled by the structures in the NMR bundle. A possible method to improve current MD forcefields is to more accurately model protein hydrophobic cores. For example, the strength of the van der Waals attraction between atoms on hydrophobic residues can be increased and the atomic sizes can be changed to those of the hard-sphere plus stereochemical constraint model. We have shown in previous studies that this model is sufficient to recapitulate side chain conformations of core residues in globular proteins [34].

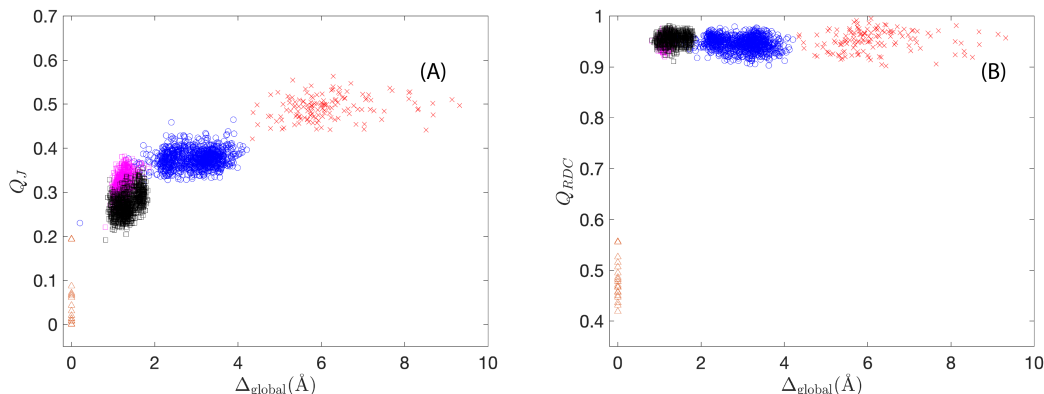


Figure 7: The deviation  $Q$  in Eq. 6 of the (A)  $^3J$ -coupling and (B) RDC values measured in NMR experiments and in MD simulations of cyclophilin A plotted versus the global  $C_\alpha$  RMSD  $\Delta_{\text{global}}$  between the structures from the MD simulations and the closest structure in the NMR bundle. Data from the NMR bundle are plotted at  $\Delta_{\text{global}} = 0$  and shown as orange triangles, and the MD simulations are indicated by black squares (Amber99SB-ILDN), magenta squares (Amber99SBNMR-ILDN), and blue circles (CHARMM36m), and the REMD simulations are represented by red crosses.

	$\langle \Delta_{\text{core}} \rangle$	$\langle \Delta_{\text{global}} \rangle$	$\langle f_{\text{NOE}} \rangle$
NMR Bundle	0.30	0.50	1.0
No restraints	1.00	2.50	$0.49 \pm 0.11$
Core restraints	0.75	1.50	$0.73 \pm 0.13$

Table 1: The first row indicates the average core  $\langle \Delta_{\text{core}} \rangle$  and global  $C_\alpha$  RMSD  $\langle \Delta_{\text{global}} \rangle$  relative to the closest NMR structure and the fraction of the NOE distance restraints  $f_{\text{NOE}}$  that are satisfied for structures in the NMR bundle for cyclophilin A. The second and third rows provide  $\langle \Delta_{\text{core}} \rangle$  and  $\langle \Delta_{\text{global}} \rangle$  from MD simulations of cyclophilin A (using the CHARMM36m forcefield) with and without NOE pairwise distance restraints between atoms belonging to core residues. For the restrained and unrestrained MD simulations of cyclophilin A, we also show the average fraction of NOE pairwise atomic separations that are satisfied for each snapshot. The error bars give the standard deviation of  $f_{\text{NOE}}$  from the average of  $10^4$  snapshots.

## 4 Methods

### 4.1 MD simulations

We used the GROMACS molecular dynamics package to carry out all of the MD and REMD simulations [35]. For cyclophilin A, the initial structures were obtained from PDB: 1oca [36] (NMR ensemble) and PDB: 3k0m [15] (x-ray crystal structure). For T4 lysozyme\*, the initial structures were obtained from PDB: 3dmv (NMR ensemble) and PDB: 2lcb (x-ray crystal structure). The proteins were solvated with TIP3P water molecules for all forcefields. Short-range van der Waals and screened Coulomb interactions were truncated at 1.2 nm, while longer-ranged electrostatics were tabulated using the Particle Mesh Ewald summation method. For cyclophilin A, the x-ray crystal structure (PDB: 3k0m) was solved at a pH of 7.5, whereas the NMR structure was solved at pH 6.5. For T4 lysozyme\*, the pH of the x-ray crystal structure (PDB:2lcb) was 6.9 and for the NMR structure, the pH was 5.5. All MD simulations in this study were performed at a pH of 7.

Two rounds of energy minimization were performed before the production simulations. The first energy

minimization relaxed the water molecules, while fixing the positions of the atoms in the protein, and the second energy minimization relaxed both the protein atoms and water molecules. In Table 2, we show how the energy minimization (using the CHARMM36m forcefield) changes the initial structure of cyclophilin A. We find that energy minimization moves the NMR models by  $\Delta_{\text{core}} \sim 0.5\text{\AA}$ . In contrast, energy minimization of the x-ray crystal structure only gives rise to  $\Delta_{\text{core}} \sim 0.02\text{\AA}$ . Also, if we apply energy minimization to an NMR structure and calculate  $\Delta_{\text{core}}$  with respect to the x-ray crystal structure, the deviation is smaller than the deviation relative to the NMR structure. Thus, energy minimization moves NMR structures toward the x-ray crystal structure. These results suggest that x-ray structures are more stable than NMR structures in the CHARMM36m forcefield[17]. We find qualitatively similar results to those in Table 2 for the two Amber forcefields, Amber99SB-ILDN [18, 19] and Amber99SBNMR-ILDN [20].

After energy minimization, we performed the MD simulations in the NPT ensemble at temperature 300K and 1 bar of isotropic pressure using the weakly coupled Berendsen thermostat and barostat, with a box size that is twice the crystal unit cell on average in each dimension and cubic periodic boundary conditions in all directions. The time constant of the Berendsen thermostat was set to 2 ps and the isothermal compressibility for the Berendsen barostat was set to  $4.5 \times 10^{-5} \text{bar}^{-1}$ . The equations of motion for the atomic coordinates and velocities were integrated using a leapfrog algorithm with a 2 fs time step. The simulations were run for 1  $\mu\text{s}$  and sampled every 100 ps. Tests for convergence of the RMSD and radius of gyration with time are discussed in Appendix 4.4.

To better sample conformation space, we also carried out replica exchange MD (REMD) simulations [37]. The REMD simulations were performed at constant NVT with the volume that gives  $P = 1$  bar at 300K using a Nosé-Hoover thermostat, with a time constant of 1 ps, a leapfrog integration algorithm, and a time step of 2fs. While the MD simulations were carried out in the NPT ensemble, NPT REMD is not implemented in the current version of GROMACS. In future studies, we will compare REMD sampling in both the NVT and NPT ensembles [38–40]. Replicas of the seed systems were duplicated and heated to temperatures ranging from 270K to 500K. The ensemble contained 89 replicas in total, such that the Markovian exchange rate between the replicas was fixed at 25%. REMD simulations were run on average for 300ns per replica. The first 100ns of the trajectories were ignored to allow for equilibration, and the following 200 ns period was analyzed.

We also performed restrained MD simulations of cyclophilin A by adding harmonic constraints between NOE atom pairs coupled with the CHARMM36m forcefield. We first identified the NOE restraints for cyclophilin A in the Biological Magnetic Resonance Data Bank (BMRB) [24]. We found that there are 4101 restraints in total and 127 restraints between atoms in core residues. For the restrained simulations, we added “pseudo-bonds” using a flat-bottom pair potential (i.e. type 10 restraints)  $V_{dr}$  between core atoms with NOE restraints. No force acts on the atom pair when its separation is within the flat region of the potential, however, a harmonic restoring force acts on the pair to move them into the flat region when the separation is outside of the flat region. The pair potential is given by the following:

$$V_{dr}(r_{ij}) = \begin{cases} \frac{k_{dr}}{2}(r_{ij} - r_0)^2, & r_{ij} < r_0 \\ 0, & r_0 \leq r_{ij} < r_1 \\ \frac{k_{dr}}{2}(r_{ij} - r_1)^2, & r_1 \leq r_{ij} < r_2 \\ \frac{k_{dr}}{2}(r_2 - r_1)(2r_{ij} - r_2 - r_1), & r_2 \leq r_{ij}, \end{cases} \quad (1)$$

where  $r_{ij}$  is the separation between NOE atom pairs,  $r_0$  and  $r_1$  are the minimum and maximum distances for the NOE atom pairs in the NMR bundle,  $r_2$  is the upper bound of the atom pair separation provided in the BMRB restraint file, and the spring constant  $k_{dr} = 10\text{kJ/mol/nm}^2$ . The spring constant is on the same order of magnitude as that for bonded heavy atoms pairs. With the restraints, we first performed energy minimization, then 2 ps of NVT equilibration, followed by an NPT production run for 1  $\mu\text{s}$ . As for the

Initial Condition	Global/Core	$\Delta(i_{\text{EM}}, j_0)$	$\Delta(i_{\text{EM}}, j_{\text{xray}})$	$\Delta(i_{\text{EM}}, j_{\text{NMR}})$
NMR	Global	0.81Å	0.21Å	0.79Å
	Core	0.47Å	0.13Å	0.43Å
x-ray	Global	0.10Å	0.10Å	0.55Å
	Core	0.02Å	0.02Å	0.39Å

Table 2: The root-mean-square deviations (RMSD)  $\Delta(i, j)$  in the positions of the  $C_\alpha$  atoms between two cyclophilin A structures:  $i$  and  $j$ . The first column indicates whether the simulation was initialized with one of the models from the NMR bundle or the x-ray crystal structure PDB: 3k0m. The second column indicates whether the  $C_\alpha$  RMSD is calculated over core residues or all residues in the protein. Three RMSD calculations were performed and displayed in the third, fourth, and fifth columns: between the energy minimized  $i_{\text{EM}}$  and initial structures  $j_0$ , between the energy minimized  $i_{\text{EM}}$  and the x-ray crystal structure  $j_{\text{xray}}$ , and the energy minimized structure  $i_{\text{EM}}$  and the structures in the NMR bundle  $j_{\text{NMR}}$ .

unrestrained MD simulations, we maintained the temperature at 300K and 1 bar of isotropic pressure using the weakly coupled Berendsen barostat and thermostat.

## 4.2 Datasets

We selected cyclophilin A from an NMR/x-ray pair dataset, which we constructed in our previous work and contains 21 proteins that have been solved by both x-ray crystallography and solution-NMR spectroscopy [11]. The NMR bundle for cyclophilin A was solved by Ottiger, *et al.* [36] (PDB: 1oca). There are 20 model structures in the bundle and all of their core residues have more than 20 NOE restraints. The x-ray crystal structure of cyclophilin A was solved by Fraser, *et al.* [15] (PDB: 3k0m) with a resolution of 1.25 Å. We also queried the PDB and found 31 duplicate x-ray crystal structures of cyclophilin A. These structures have resolution  $< 2\text{Å}$  and the sequence similarity is greater than 95% compared to the structure with PDB:3k0m. To consider the generality of our results for cyclophilin A, we also performed MD simulations of T4 lysozyme\* (which is a mutant of T4 lysozyme with four point mutations, R12G, C55T, C97A, and I137R). This particular mutant has both high quality x-ray and NMR structures. The x-ray crystal structure for T4 lysozyme\* was solved by Liu, *et al.* [16] (PDB:3dmv) at resolution 1.65 Å and the NMR ensemble was determined by Bouvignies, *et al.* [41] (PDB:2lcb) with 6 model structures. We also identified 9 x-ray crystal duplicate structures for T4 lysozyme\* with resolution  $< 2\text{Å}$  and sequence similarity  $> 95\%$  compared to the x-ray crystal structure with PDB:3dmv.

For the analyses of the MD and REMD simulations, each protein conformation was pre-processed using the REDUCE software package, which sets the bond lengths for C-H, N-H, and S-H to 1.1, 1.0, and 1.3 Å and the bond angles to  $109.5^\circ$  and  $120^\circ$  for hydrogen bond angles involving the  $C_{\text{sp}3}$  and  $C_{\text{sp}2}$  atoms, respectively [42]. We also set the values for the atomic radii to be the following:  $C_{\text{sp}3}$ :1.5Å;  $C_{\text{O}}$ : 1.3Å; O: 1.4Å; N:1.3Å;  $H_{\text{C}}$ :1.10Å;  $H_{\text{O,N}}$ :1.00Å, and S:1.75Å, which were obtained in prior work by minimizing the difference between the side-chain dihedral angle distributions predicted by the hard-sphere dipeptide mimetic model and those observed in protein crystal structures for a subset of amino acid types [43]. Using these atomic radii, we quantified the relative solvent accessible surface area and the number and packing fraction of core residues.



### 4.3 Root-mean-square deviations

We measured the root-mean-square deviation (RMSD) of the  $C_\alpha$  atom positions between two structures  $i$  and  $j$  after alignment:

$$\Delta(i, j) = \sqrt{\frac{1}{N_s} \sum_{\mu=1}^{N_s} (\vec{c}_{\mu,j} - \vec{c}_{\mu,i})^2}, \quad (2)$$

where  $\vec{c}_{\mu,j}$  is the position of the  $C_\alpha$  atom on residue  $\mu$  in structure  $i$ , and  $N_s$  is the total number of residues that are being compared on the two structures.

We calculated both the core and global  $C_\alpha$  RMSD ( $\Delta_{\text{core}}$  and  $\Delta_{\text{global}}$ ) between structure pairs. To calculate the core RMSD, we used the core residues to both align and then compute the RMSD between the two structures. (Identification of core residues is discussed in Sec. 4.3.1.) Between the experimental structure pairs (NMR/NMR, x-ray/x-ray, and NMR/x-ray) the set of core residues varies by  $\lesssim 20\%$ , therefore, we use the union of core residues in both structures. When an MD conformation is compared to an experimental structure, we use the set of core residues defined in the experimental structure. When calculating global RMSD, we align the structures excluding the first and last 4 amino acids. In addition, when we report the RMSD between an MD conformation and structures in the NMR bundle, we first calculate the RMSD between the MD conformation and each structure in the NMR bundle, as all structures in the NMR bundle are equally valid. Then, we report the minimum RMSD in this set. The Biopython package was used to align the structures and calculate the RMSD [44, 45].

#### 4.3.1 Relative solvent accessible surface area

To identify core residues, we measured each residue’s solvent accessible surface area (SASA). To calculate SASA, we use the NACCESS software package [46], which implements an algorithm originally proposed by Lee and Richards [47]. The algorithm takes z-slices of the protein, determines the solvent accessibility of the sets of contours using a probe molecule of a given radius, and integrates the SASA over the slices. We use a water-molecule-sized probe with radius  $1.4 \text{ \AA}$  and z-slices with thickness  $\Delta z = 10^{-3} \text{ \AA}$ , which were used in previous work [11, 14, 34, 48, 49]. To normalize the SASA, we take the ratio of the SASA within the context of the protein ( $\text{SASA}_{\text{context}}$ ) and the SASA of the same residue  $X$  extracted from the protein structure as a dipeptide (Gly-X-Gly) with the same backbone and side-chain dihedral angles:

$$\text{rSASA} = \frac{\text{SASA}_{\text{context}}}{\text{SASA}_{\text{dipeptide}}}. \quad (3)$$

Core residues are classified as those that have  $\text{rSASA} \leq 10^{-3}$ . This is the largest value of rSASA such that the packing fraction and side-chain repacking predictability no longer depend on the value of the rSASA cutoff when it is decreased.

#### 4.3.2 Packing fraction

A characteristic measure of the packing efficiency of a system is the dimensionless volume fraction, or packing fraction. The packing fraction of residue  $\mu$  is

$$\phi_\mu = \frac{v_\mu}{V_\mu}, \quad (4)$$

where  $v_\mu$  is the non-overlapping volume of residue  $\mu$  and  $V_\mu$  is the volume of the surface Voronoi volume of residue  $\mu$ . To calculate the Voronoi tessellation for a given protein core, we employ surface Voronoi tessellation [50], which defines a Voronoi cell as the region of space that is closer to the bounding surface of

residue  $\mu$  than to the bounding surface of any other residue in the protein. We calculate the surface Voronoi tessellation using POMELO software package [51]. This software approximates the bounding surfaces of each residue by triangulating points on the residue surfaces. We find that using  $\sim 400$  points per atom, or  $\sim 6400$  surface points per residue, gives an accurate representation of the surface Voronoi cells and the results do not change if more surface points are included.

#### 4.4 Comparison of NMR structures to those generated by MD simulations

We compared the conformations generated from the MD simulations to NMR measurements in several ways. In particular, we computed  $^3J$ -coupling constants using the Karplus equation and we calculated residual dipolar couplings (RDCs) using the PALES software [29].  $^3J$ -coupling constants are determined by the dihedral angle among the two coupled nuclei and the two heavy atoms on either side. For example, the backbone dihedral angle  $\phi$  among the backbone atoms C-N-C $_{\alpha}$ -C determines  $^3J_{H_N H_{C_{\alpha}}}$ . To compute the  $^3J_{H_N H_{C_{\alpha}}}$  coupling constants from the MD simulations, we used the Karplus equation:

$$^3J_{H_N H_{C_{\alpha}}}(\phi) = A \cos^2(\phi + \Theta) + B \cos(\phi + \Theta) + C, \quad (5)$$

where  $\Theta$  is the phase shift, and  $A$ ,  $B$ , and  $C$  are constants. We used the parameterization of Hu and Bax [52]:  $A = 7.09$  Hz,  $B = -1.42$  Hz,  $C = 1.55$  Hz, and  $\Theta = -60^\circ$ . Although there are other parameter sets, the correlation between MD simulation and experimental  $^3J$  couplings are insensitive to the specific choice of the Karplus parameters [52]. Also, a single set of Karplus parameters can be applied equally well to all residue types.

To compare the experimental and calculated values of the NMR measurements, we computed the deviation:

$$Q_S = \frac{\sqrt{N_m^{-1} \sum_{i=1}^{N_m} (S_i^{\text{calc}} - S_i^{\text{exp}})^2}}{\sqrt{N_m^{-1} \sum_{i=1}^{N_m} (S_i^{\text{exp}})^2}}, \quad (6)$$

where the sum is over the  $N_m$  available measurements of the quantity  $S$  (i.e. either the  $^3J$ -couplings or RDCs),  $S_i^{\text{exp}}$  is the experimental value, and  $S_i^{\text{calc}}$  is calculated from the structure's atomic coordinates [30].

## Acknowledgments

The authors acknowledge support from NIH Training Grant No. T32GM008283 (A.T.G.) and T32EB019941 (J.D.T.), the Integrated Graduate Program in Physical and Engineering Biology (Z.M.), NSF Grant Nos. DBI-1755494 (G.M.C.), PHY-1522467 (C.S.O), and PHY-2012406 (C.S.O), as well as Fortum Foundation (M.V.), Academy of Finland Grant No. 309324 (M.S.), CSC-IT Centre for Science Ltd. Finland (M.V.). Computational resources were provided by an XSEDE research allocation award No. MCB190047. This work also benefited from the facilities and staff of the Yale University Faculty of Arts and Sciences High Performance Computing Center.

## Data Availability

The data that support the findings of this study are available from the corresponding author upon reasonable request.

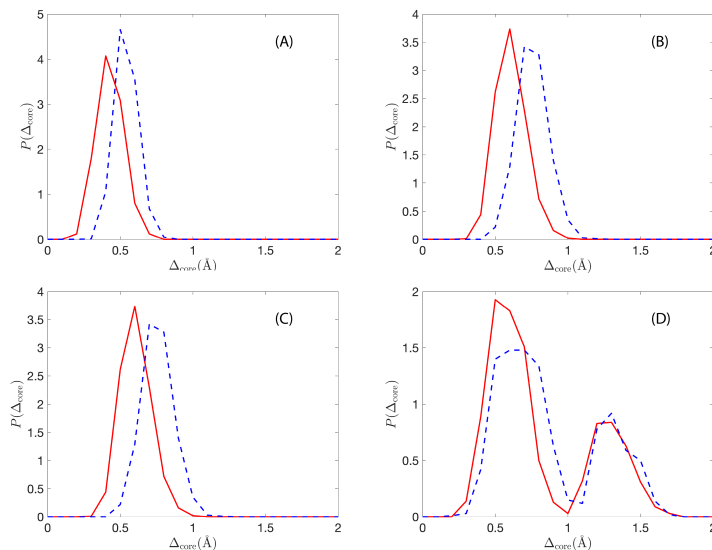


Figure 8: Probability distributions of the core  $C_\alpha$  RMSD  $P(\Delta_{\text{core}})$  from MD simulations of cyclophilin A using the (A) Amber99SBNMR-ILDN forcefield and (B) Amber99SB-ILDN forcefields starting from the x-ray crystal structure PDB: 3k0m.  $P(\Delta_{\text{core}})$  from MD simulations of cyclophilin A using the (C) Amber99SBNMR-ILDN and (D) Amber99SB-ILDN forcefields starting from one of the structures in the NMR bundle (PDB code: 1oca). In all panels, the core  $C_\alpha$  RMSD is calculated relative to the NMR structure that gives the minimum  $\Delta_{\text{core}}$  (blue dashed lines) or relative to the x-ray crystal structure PDB: 3k0m (red solid lines). (See Fig. 2 (C)-(D) for similar results using the CHARMM36m forcefield).

## Appendix A: MD simulations of cyclophilin A with different initial conditions

In this Appendix, we show that the core RMSD from MD simulations of cyclophilin A initiated from multiple structures in the NMR bundle are smaller when calculated relative to the x-ray crystal structure PDB: 3k0m compared to when calculated relative to the NMR bundle. In Fig. 2 (C)-(D), we showed this result for the CHARMM36m forcefield. In Fig. 8, we show similar results for the Amber99SB-ILDN and Amber99SBNMR-ILDN forcefields.

## Appendix B: Testing convergence of MD simulations

To assess the convergence of the MD simulations, we calculated the average core and global  $C_\alpha$  RMSD,  $\langle \Delta_{\text{core}} \rangle$  and  $\langle \Delta_{\text{global}} \rangle$ , as well as the average radius of gyration  $\langle R_g \rangle$ , for cyclophilin A as a function of time. For the two Amber forcefields, both  $\langle \Delta_{\text{core}} \rangle$  and  $\langle \Delta_{\text{global}} \rangle$  plateau after  $\sim 100$ ns as shown in Fig. 9 (B) and (C). In contrast, for the CHARMM36m forcefield, the core RMSD plateaus, but  $\langle \Delta_{\text{global}} \rangle$  continues to increase beyond 1000ns. (See Fig. 9 (A).) We find the same results for  $\langle R_g \rangle$  versus time in Fig. 9 (D)-(F), indicating that longer-time MD simulations of cyclophilin A using CHARMM36m will lead to partial unfolding, whereas the MD simulations using the two Amber forcefields are stationary in time. As a result, we do not carry out MD simulations of cyclophilin A longer than  $1\mu\text{s}$ , and instead use REMD simulations to explore additional conformations for cyclophilin A.

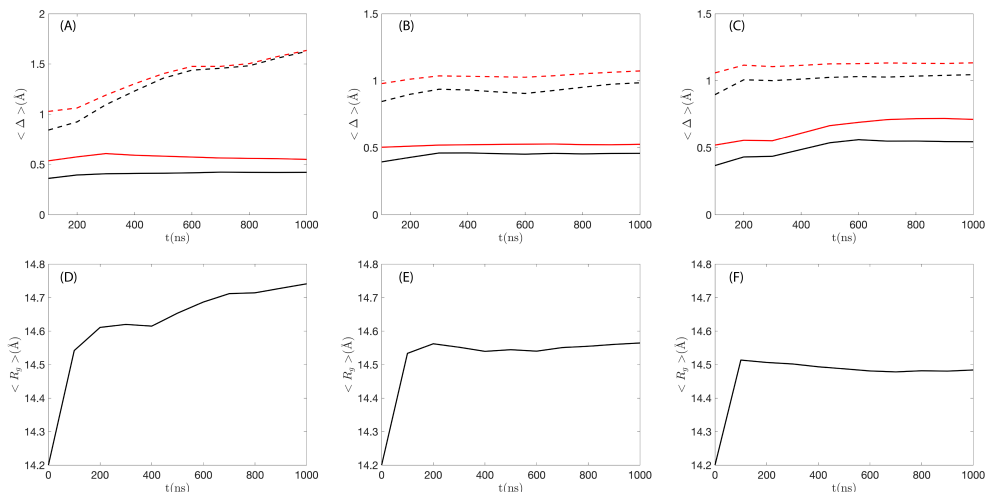


Figure 9: The core and global  $C_\alpha$  RMSD,  $\Delta_{\text{core}}$  (solid lines) and  $\Delta_{\text{global}}$  (dotted lines) as a function of time  $t$  from MD simulations of cyclophilin A averaged over frames from 0 to  $t$  for the (A) CHARMM36m, (B) Amber99SB-ILDN, and (C) Amber99SBNMR-ILDN forcefields. The RMSD of the protein conformations are calculated relative to NMR bundle (red lines) and x-ray crystal structure (black lines). Similar data is also shown for the average radius of gyration  $R_g$  as a function of time for (D) CHARMM36m, (E) Amber99SB-ILDN, and (F) Amber99SBNMR-ILDN.

## Appendix C: MD simulations of protein folding and stability

In this Appendix, we provide a summary of all-atom MD simulations of globular protein folding starting from non-native conformations and globular protein stability starting from experimentally-determined structures. Overall, most folding simulations have been conducted on small proteins containing less than 80 residues. Simulations of protein stability have been performed on larger proteins, but none larger than the proteins considered in the present studies.

### 4.5 Folding simulations

We identified 15 globular proteins that have been folded from their primary structures using all-atom MD simulations as shown in Table 3. These proteins range from 10-80 amino acids and they all have relatively short folding times ( $< 1\mu\text{s}$ ). Proteins with  $\lesssim 35$  residues have been folded within  $\Delta_{\text{global}} \sim 1\text{\AA}$  of the experimentally-determined structure. For larger proteins,  $\Delta_{\text{global}}$  begins to increase, reaching  $\sim 5\text{\AA}$  for some proteins with more than 55 residues. In contrast,  $\Delta_{\text{global}} \sim 1-2\text{\AA}$  for high-quality NMR bundles [11].

### 4.6 Stability simulations

We identified a number of prior MD simulations of protein stability, where the experimentally-determined structures are used as initial conditions in the MD simulations in explicit solvent at room temperature. These prior studies have characterized the conformational fluctuations in 19 distinct proteins ranging in size from 48-224 amino acids. Some of these MD simulations are listed in Table 4 and others are provided in Table S20 in Robustelli, *et al.* [13]. The range of the total simulation times varies broadly, from 1ns to  $10\mu\text{s}$ . The average global  $C_\alpha$  RMSD  $\Delta_{\text{global}} > 1\text{\AA}$  for all of the MD simulations. In Robustelli, *et al.* [13], the authors carried out  $20\mu\text{s}$  MD simulations for 14 proteins using six different forcefields. Only one of the

Protein	$N$	$\Delta_{\text{global}}(\text{\AA})$	Expts	Forcefields	Reference
Chignolin	10	1.0	NMR	C22	[53]
CLN025	10	0.9	NMR	A11	[54]
Trp-Cage	20	1.4	NMR	C22	[53]
Trp-Cage	20	1.7	NMR	A11	[54]
BBA	28	1.6	NMR	C22	[53]
Villin	35	1.3	x-ray	C22	[53]
WW-DOMAIN	35	1.2	x-ray	C22	[53]
NTL9	39	0.5	x-ray	C22	[53]
NTL9	39	3.0	x-ray	Gromos	[55]
NTL9	39	1 – 2	x-ray	A99SB-ILDN	[56]
BBL	47	1.2	NMR	C22	[53]
Protein B	47	3.3	NMR	C22	[53]
Homeodomain	52	3.6	NMR	C22	[53]
Protein G	56	4.8	x-ray	C22	[53]
A3D	73	4.8	NMR	C22	[53]
$\lambda$ -repressor	80	1.8	x-ray	C22	[53]

Table 3: Globular proteins longer than 10 amino acids that have been folded from their primary structure using MD simulations with specified forcefields. The column “Expts” reports the experimental method used to solve the protein structure and the global  $C_{\alpha}$  RMSD of the MD conformations was calculated relative to this type of experimental structure. Amber is abbreviated as “A” and CHARMM is abbreviated as “C”.

14 proteins was determined via NMR spectroscopy, the rest were characterized using x-ray crystallography with a resolution  $\leq 2.3\text{\AA}$ . Amber99SB\*-ILDN with TIP3P showed the best performance, with an average RMSD over the final  $1\mu\text{s}$  of each simulation across all 14 proteins of  $2.1\text{\AA}$ .

## Appendix D: Restrained simulations

To carry out the restrained MD simulations, we obtained information about the NOE restraints from the BRMD website, <https://bmr.io>. In the restrained MD simulations, we applied harmonic constraints between 127 pairs of core atoms. In this Appendix, we list 23 of the atom pairs, i.e. those that involve core heavy atoms, in Table 5.

## References

- [1] Helen M. Berman, John Westbrook, Zukang Feng, Gary Gilliland, T. N. Bhat, Helge Weissig, Ilya N. Shindyalov, and Philip E. Bourne. The Protein Data Bank. *Nucleic Acids Research*, 28(1):235–242, 01 2000.
- [2] Stephen K Burley, Helen M Berman, Charmi Bhikadiya, Chunxiao Bi, Li Chen, Luigi Di Costanzo, Cole Christie, Ken Dalenberg, Jose M Duarte, Shuchismita Dutta, Zukang Feng, Sutapa Ghosh, David S Goodsell, Rachel K Green, Vladimir Guranović, Dmytro Guzenko, Brian P Hudson, Tara Kalro, Yuhe Liang, Robert Lowe, Harry Namkoong, Ezra Peisach, Irina Periskova, Andreas Prlić, Chris Randle, Alexander Rose, Peter Rose, Raul Sala, Monica Sekharan, Chenchua Shao, Lihua Tan, Yi-Ping Tao, Yana Valasatava, Maria Voigt, John Westbrook, Jesse Woo, Huanwang Yang, Jasmine

Protein	$N$	x-ray/NMR	Forcefield	$\Delta_{\text{global}}(\text{\AA})$	Ref.
Crambin	46	x-ray	C36m	$\sim 0.75$	[17]
Homeodomain	52	NMR	ENCAD	3.58	[57]
GB3	56	x-ray	A99SB-ILDN	1.3	[58]
			C36m	$\sim 0.9$	[17]
			OPLS	1.0	[59]
			A03	$\sim 2.0$	[25]
			A99sb	$\sim 1.75$	[25]
BPTI	58	x-ray	C36m	1.75	[17]
Erabutoxin B	62	x-ray	C36m	2.0	[17]
CSPA	69	x-ray	C36m	1.8	[17]
Ubiquitin	76	x-ray	A99SB-ILDN	1.07	[60]
			OPLS	1.0	[59]
			C36m	$\sim 2.0$	[17]
Apomyoglobin	153	x-ray	GAFF	2.50	[61]
RAP74 C-term	73	x-ray	C36m	$\sim 3.0$	[17]
Trimmed ribo-S6	74	x-ray	C36m	$\sim 1.75$	[17]
DMAP1	75	x-ray	C36m	$\sim 1.0$	[17]
ICaBP	75	x-ray	C36m	$\sim 3.5$	[17]
PDZ	85	x-ray	C36m	$\sim 1.1$	[17]
TEL	129	x-ray	C36m	$\sim 2.0$	[17]
FABP	131	x-ray	C36m	$\sim 1.5$	[17]
DroHb	153	x-ray	A14SB	$\sim 1.0$	[62]
Mb	153	x-ray	C36m	$\sim 2.5$	[17]
DTB Syn	224	x-ray	C36m	$\sim 2.0$	[17]

Table 4: MD simulations of proteins for which the experimental structures (with the method given in the third column) are used as the initial conditions. The global  $C_{\alpha}$  RMSD of the conformations in the MD simulations are calculated relative to the experimental structure indicated in the third column. Amber is abbreviated as “A” and CHARMM is abbreviated as “C.”

Young, Marina Zhuravleva, and Christine Zardecki. RCSB Protein Data Bank: biological macromolecular structures enabling research and education in fundamental biology, biomedicine, biotechnology and energy. *Nucleic Acids Research*, 47(D1):D464–D474, 10 2018.

- [3] John Moult, Krzysztof Fidelis, Andriy Kryshtafovych, Torsten Schwede, and Anna Tramontano. Critical assessment of methods of protein structure prediction: Progress and new directions in Round XI. *Proteins: Structure, Function, and Bioinformatics*, 84(S1):4–14, 2016.
- [4] John Moult, Krzysztof Fidelis, Andriy Kryshtafovych, Torsten Schwede, and Anna Tramontano. Critical assessment of methods of protein structure prediction (CASP)—Round XII. *Proteins: Structure, Function, and Bioinformatics*, 86(S1):7–15, 2018.
- [5] Andriy Kryshtafovych, Torsten Schwede, Maya Topf, Krzysztof Fidelis, and John Moult. Critical assessment of methods of protein structure prediction (CASP)—Round XIII. *Proteins: Structure, Function, and Bioinformatics*, 87(12):1011–1020, 2019.
- [6] Xavier Daura, Bernhard Jaun, Dieter Seebach, Wilfred F van Gunsteren, and Alan E Mark. Reversible

ResID	Res Type	Atom	Res ID	Res Type	Atom
6	VAL	CG1	22	PHE	CD1
6	VAL	CG1	22	PHE	CD2
6	VAL	CG2	22	PHE	CD1
6	VAL	CG2	22	PHE	CE1
6	VAL	CG2	24	LEU	CD2
6	VAL	CG2	98	LEU	CD1
22	PHE	CD1	98	LEU	CD1
22	PHE	CD1	98	LEU	CD2
22	PHE	CE1	98	LEU	CD2
22	PHE	CE1	98	LEU	CE1
22	PHE	CE1	98	LEU	CD2
24	LEU	CD1	129	PHE	CE1
24	LEU	CD2	98	LEU	CD1
24	LEU	CD2	98	LEU	CD2
24	LEU	CD2	130	GLY	CA
56	ILE	CG1	62	CYS	CB
62	CYS	CB	139	VAL	CG1
98	LEU	CD1	112	PHE	CB
98	LEU	CD1	112	PHE	CD1
98	LEU	CD1	129	PHE	CE1
98	LEU	CD1	130	GLY	CA
98	LEU	CD2	112	PHE	CB
98	LEU	CD2	112	PHE	CD1
98	LEU	CD2	129	PHE	CE1

Table 5: The 24 atomic pairs in cyclophilin A for which both atoms are in core residues and NOE restraints have been measured. The atom types are reported in PDB format:  $C_\alpha$  (CA),  $C_\beta$  (CB),  $C_\gamma$  (CG),  $C_\delta$  (CD), and  $C_\epsilon$  (CE).

peptide folding in solution by molecular dynamics simulation. *Journal of Molecular Biology*, 280(5): 925–932, 1998.

- [7] Michael Schaefer, Christian Bartels, and Martin Karplus. Solution conformations and thermodynamics of structured peptides: Molecular dynamics simulation with an implicit solvation model. *Journal of Molecular Biology*, 284(3):835–848, 1998.
- [8] Philippe Ferrara, Joannis Apostolakis, and Amedeo Caflisch. Thermodynamics and kinetics of folding of two model peptides investigated by molecular dynamics simulations. *The Journal of Physical Chemistry B*, 104(20):5000–5010, 05 2000.
- [9] Bosco K Ho and Ken A Dill. Folding very short peptides using molecular dynamics. *PLOS Computational Biology*, 2(4):1–10, 04 2006.
- [10] Elio A. Cino, Wing-Yiu Choy, and Mikko Karttunen. Comparison of secondary structure formation using 10 different force fields in microsecond molecular dynamics simulations. *Journal of Chemical Theory and Computation*, 8(8):2725–2740, 08 2012.
- [11] Zhe Mei, John D. Treado, Alex T. Grigas, Zachary A. Levine, Lynne Regan, and Corey S. O’Hern.

- Analyses of protein cores reveal fundamental differences between solution and crystal structures. *Proteins: Structure, Function, and Bioinformatics*, 88(9):1154–1161, 2020.
- [12] Sergiy O. Garbuzynskiy, Bogdan S. Melnik, Michail Yu. Lobanov, Alexei V. Finkelstein, and Oxana V. Galzitskaya. Comparison of x-ray and nmr structures: Is there a systematic difference in residue contacts between x-ray- and nmr-resolved protein structures? *Proteins: Structure, Function, and Bioinformatics*, 60(1):139–147, 2005.
  - [13] Paul Robustelli, Stefano Piana, and David E. Shaw. Developing a molecular dynamics force field for both folded and disordered protein states. *Proceedings of the National Academy of Sciences*, 115(21):E4758–E4766, 2018.
  - [14] Alex T. Grigas, Zhe Mei, John D. Treado, Zachary A. Levine, Lynne Regan, and Corey S. O’Hern. Using physical features of protein core packing to distinguish real proteins from decoys. *Protein Science*, 29(9):1931–1944, 2020.
  - [15] James S. Fraser, Michael W. Clarkson, Sheena C. Degnan, Renske Erion, Dorothee Kern, and Tom Alber. Hidden alternative structures of proline isomerase essential for catalysis. *Nature*, 462(7273):669–673, 2009.
  - [16] Lijun Liu, Walter A. Baase, and Brian W. Matthews. Halogenated benzenes bound within a non-polar cavity in T4 lysozyme provide examples of  $I \cdots S$  and  $I \cdots Se$  halogen-bonding. *Journal of Molecular Biology*, 385(2):595–605, 2009.
  - [17] Jing Huang, Sarah Rauscher, Grzegorz Nawrocki, Ting Ran, Michael Feig, Bert L de Groot, Helmut Grubmüller, and Alexander D MacKerell. CHARMM36m: An improved force field for folded and intrinsically disordered proteins. *Nature Methods*, 14(1):71–73, 2017.
  - [18] Robert B. Best and Gerhard Hummer. Optimized molecular dynamics force fields applied to the helix-coil transition of polypeptides. *The Journal of Physical Chemistry B*, 113(26):9004–9015, 07 2009.
  - [19] Kresten Lindorff-Larsen, Stefano Piana, Kim Palmo, Paul Maragakis, John L. Klepeis, Ron O. Dror, and David E. Shaw. Improved side-chain torsion potentials for the Amber ff99SB protein force field. *Proteins: Structure, Function, and Bioinformatics*, 78(8):1950–1958, 2010.
  - [20] Da-Wei Li and Rafael Brüschweiler. NMR-based protein potentials. *Angewandte Chemie International Edition*, 49(38):6778–6780, 2010.
  - [21] Karolis Uziela, Nanjiang Shu, Björn Wallner, and Arne Elofsson. ProQ3: Improved model quality assessments using rosetta energy terms. *Scientific Reports*, 6:33509, 10 2016.
  - [22] Rin Sato and Takashi Ishida. Protein model accuracy estimation based on local structure quality assessment using 3d convolutional neural network. *PLOS ONE*, 14(9):1–15, 09 2019.
  - [23] Mikhail Karasikov, Guillaume Pagès, and Sergei Grudinin. Smooth orientation-dependent scoring function for coarse-grained protein quality assessment. *Bioinformatics*, 35(16):2801–2808, 12 2018.
  - [24] Eldon L. Ulrich, Hideo Akutsu, Jurgen F. Doreleijers, Yoko Harano, Yannis E. Ioannidis, Jundong Lin, Miron Livny, Steve Mading, Dimitri Maziuk, Zachary Miller, Eiichi Nakatani, Christopher F. Schulte, David E. Tolmie, R. Kent Wenger, Hongyang Yao, and John L. Markley. Biomagresbank. *Nucleic Acids Research*, 36:D402–D408, 11 2007.



- [25] Oliver F. Lange, David van der Spoel, and Bert L. de Groot. Scrutinizing molecular mechanics force fields on the submicrosecond timescale with nmr data. *Biophysical Journal*, 99(2):647 – 655, 2010.
- [26] Robert B. Best, Nicolae-Viorel Buchete, and Gerhard Hummer. Are current molecular dynamics force fields too helical? *Biophysical Journal*, 95(1):L07 – L09, 2008.
- [27] Kyle A. Beauchamp, Yu-Shan Lin, Rhiju Das, and Vijay S. Pande. Are protein force fields getting better? a systematic benchmark on 524 diverse nmr measurements. *Journal of Chemical Theory and Computation*, 8(4):1409–1414, 04 2012.
- [28] Kresten Lindorff-Larsen, Paul Maragakis, Stefano Piana, Michael P. Eastwood, Ron O. Dror, and David E. Shaw. Systematic validation of protein force fields against experimental data. *PLoS ONE*, 7(2):1–6, 02 2012.
- [29] Markus Zweckstetter. NMR: prediction of molecular alignment from structure using the pales software. *Nature Protocols*, 3(4):679–690, 2008.
- [30] Gabriel Cornilescu, John L. Marquardt, Marcel Ottiger, and Ad Bax. Validation of protein structure from anisotropic carbonyl chemical shifts in a dilute liquid crystalline phase. *Journal of the American Chemical Society*, 120(27):6836–6837, 06 1998.
- [31] Marcel Ottiger and Ad Bax. Bicelle-based liquid crystals for NMR-measurement of dipolar couplings at acidic and basic pH values. *Journal of Biomolecular NMR*, 13(2):187–191, 1999.
- [32] Carlo Camilloni, Aleksandr B. Sahakyan, Michael J. Holliday, Nancy G. Isern, Fengli Zhang, Elan Z. Eisenmesser, and Michele Vendruscolo. Cyclophilin A catalyzes proline isomerization by an electrostatic handle mechanism. *Proceedings of the National Academy of Sciences*, 111(28):10203–10208, 2014.
- [33] Scott A. Showalter and Rafael Brüschweiler. Quantitative molecular ensemble interpretation of NMR dipolar couplings without restraints. *Journal of the American Chemical Society*, 129(14):4158–4159, 04 2007.
- [34] J. C. Gaines, A. Virrueta, D. A. Buch, S. J. Fleishman, C. S. O’Hern, and L. Regan. Collective repacking reveals that the structures of protein cores are uniquely specified by steric repulsive interactions. *Protein Engineering, Design and Selection*, 30(5):387–394, 02 2017.
- [35] Mark James Abraham, Teemu Murtola, Roland Schulz, Szilárd Páll, Jeremy C. Smith, Berk Hess, and Erik Lindahl. Gromacs: High performance molecular simulations through multi-level parallelism from laptops to supercomputers. *SoftwareX*, 1-2:19–25, 2015.
- [36] Marcel Ottiger, Oliver Zerbe, Peter Güntert, and Kurt Wüthrich. The NMR solution conformation of unligated human cyclophilin A. *Journal of Molecular Biology*, 272(1):64 – 81, 1997.
- [37] Yuji Sugita and Yuko Okamoto. Replica-exchange molecular dynamics method for protein folding. *Chemical Physics Letters*, 314(1):141–151, 1999.
- [38] Tsuneyasu Okabe, Masaaki Kawata, Yuko Okamoto, and Masuhiro Mikami. Replica-exchange Monte Carlo method for the isobaric–isothermal ensemble. *Chemical Physics Letters*, 335(5):435–439, 2001.
- [39] Edyta Małolepsza, Maxim Secor, and Tom Keyes. Isobaric molecular dynamics version of the generalized replica exchange method (gREM): Liquid–vapor equilibrium. *The Journal of Physical Chemistry B*, 119(42):13379–13384, 10 2015.

- [40] Masataka Yamauchi and Hisashi Okumura. Development of isothermal-isobaric replica-permutation method for molecular dynamics and Monte Carlo simulations and its application to reveal temperature and pressure dependence of folded, misfolded, and unfolded states of chignolin. *The Journal of Chemical Physics*, 147(18):184107, 2017.
- [41] Guillaume Bouvignies, Pramodh Vallurupalli, D. Flemming Hansen, Bruno E. Correia, Oliver Lange, Alaji Bah, Robert M. Vernon, Frederick W. Dahlquist, David Baker, and Lewis E. Kay. Solution structure of a minor and transiently formed state of a T4 lysozyme mutant. *Nature*, 477(7362):111–114, 2011.
- [42] J. Michael Word, Simon C. Lovell, Jane S. Richardson, and David C. Richardson. Asparagine and glutamine: Using hydrogen atom contacts in the choice of side-chain amide orientation. *Journal of Molecular Biology*, 285(4):1735–1747, 1999.
- [43] Alice Qinhua Zhou, Corey S. O’Hern, and Lynne Regan. The power of hard-sphere models: Explaining side-chain dihedral angle distributions of Thr and Val. *Biophysical Journal*, 102(10):2345–2352, 2012.
- [44] Thomas Hamelryck and Bernard Manderick. PDB file parser and structure class implemented in Python. *Bioinformatics*, 19(17):2308–2310, 11 2003.
- [45] Peter J. A. Cock, Tiago Antao, Jeffrey T. Chang, Brad A. Chapman, Cymon J. Cox, Andrew Dalke, Iddo Friedberg, Thomas Hamelryck, Frank Kauff, Bartek Wilczynski, and Michiel J. L. de Hoon. Biopython: Freely available Python tools for computational molecular biology and bioinformatics. *Bioinformatics*, 25(11):1422–1423, 03 2009.
- [46] S. J. Hubbard and J. M. Thornton. Naccess, 1993.
- [47] B. Lee and F. M. Richards. The interpretation of protein structures: Estimation of static accessibility. *Journal of Molecular Biology*, 55(3):379–400, 1971.
- [48] Jennifer C. Gaines, W. Wendell Smith, Lynne Regan, and Corey S. O’Hern. Random close packing in protein cores. *Physical Review E*, 93:032415, 2016.
- [49] John D. Treado, Zhe Mei, Lynne Regan, and Corey S. O’Hern. Void distributions reveal structural link between jammed packings and protein cores. *Physical Review E*, 99:022416, 2019.
- [50] Fabian M. Schaller, Sebastian C. Kapfer, Myfanwy E. Evans, Matthias J.F. Hoffmann, Tomaso Aste, Mohammad Saadatfar, Klaus Mecke, Gary W. Delaney, and Gerd E. Schröder-Turk. Set voronoi diagrams of 3D assemblies of aspherical particles. *Philosophical Magazine*, 93(31-33):3993–4017, 2013.
- [51] Simon Weis, Philipp W. A. Schönhöfer, Fabian M. Schaller, Matthias Schröter, and Gerd E. Schröder-Turk. Pomelo, a tool for computing generic set Voronoi diagrams of aspherical particles of arbitrary shape. *EPJ Web of Conferences*, 140:06007, 2017.
- [52] Jin-Shan Hu and Ad Bax. Determination of  $\phi$  and  $\chi_1$  angles in proteins from  $^{13}\text{C}$ – $^{13}\text{C}$  three-bond J couplings measured by three-dimensional heteronuclear NMR. How planar is the peptide bond? *Journal of the American Chemical Society*, 119(27):6360–6368, 07 1997.
- [53] Kresten Lindorff-Larsen, Stefano Piana, Ron O. Dror, and David E. Shaw. How fast-folding proteins fold. *Science*, 334(6055):517–520, 2011.

- [54] Yuan-Ping Pang. How fast fast-folding proteins fold in silico. *Biochemical and Biophysical Research Communications*, 492(1):135–139, 2017.
- [55] Anna S. Kamenik, Philip H. Handle, Florian Hofer, Ursula Kahler, Johannes Kraml, and Klaus R. Liedl. Polarizable and non-polarizable force fields: Protein folding, unfolding, and misfolding. *The Journal of Chemical Physics*, 153(18):185102, 2020.
- [56] Wei Chen, Chuanyin Shi, Alexander D. MacKerell, and Jana Shen. Conformational dynamics of two natively unfolded fragment peptides: Comparison of the amber and charmm force fields. *The Journal of Physical Chemistry B*, 119(25):7902–7910, 2015.
- [57] Michael Levitt, Miriam Hirshberg, Ruth Sharon, and Valerie Daggett. Potential energy function and parameters for simulations of the molecular dynamics of proteins and nucleic acids in solution. *Computer Physics Communications*, 91(1):215–231, 1995.
- [58] Tong Li, Qingqing Jing, and Lishan Yao. Dynamics of the GB3 loop regions from MD simulation: How much of it is real? *The Journal of Physical Chemistry B*, 115(13):3488–3495, 2011.
- [59] Michael J. Robertson, Julian Tirado-Rives, and William L. Jorgensen. Improved peptide and protein torsional energetics with the opls-aa force field. *Journal of Chemical Theory and Computation*, 11(7): 3499–3509, 07 2015.
- [60] Assaf Ganoth, Yossi Tsfadia, and Reuven Wiener. Ubiquitin: Molecular modeling and simulations. *Journal of Molecular Graphics and Modelling*, 46:29–40, 2013.
- [61] Dawei Zhang and Raudah Lazim. Application of conventional molecular dynamics simulation in evaluating the stability of apomyoglobin in urea solution. *Scientific Reports*, 7(1):44651, 2017.
- [62] Laia JulióPlana, Alejandro D. Nadra, Dario A. Estrin, F. Javier Luque, and Luciana Capece. Thermal stability of globins: Implications of flexibility and heme coordination studied by molecular dynamics simulations. *Journal of Chemical Information and Modeling*, 59(1):441–452, 01 2019.